

Article

The Electrochemical Detection of Bisphenol A and Catechol in Red Wine

Chao Wang^{1,2}, Xiangchuan Wu³, Xinhe Lin³, Xueting Zhu³, Wei Ma^{1,2,*} and Jian Chen^{1,2,*}

¹ School of Biotechnology, Jiangnan University, Wuxi 214000, China; wangchao@jiangnan.edu.cn (C.W.); wei.ma@jiangnan.edu.cn (W.M.)

² Science Center for Future Foods, Jiangnan University, Wuxi 210023, China

³ School of Food Science and Pharmaceutical Engineering, Nanjing Normal University, Nanjing 210023, China; wxyaxxx@163.com (X.W.); 18068849373@163.com (X.L.); 13913931306@163.com (X.Z.)

* Correspondence: jchen@jiangnan.edu.cn

Abstract: The use of nanozymes for electrochemical detection in the food industry is an intriguing area of research. In this study, we synthesized a laccase mimicking the MnO₂@CeO₂ nanozyme using a simple hydrothermal method, which was characterized by modern analytical methods, such as transmission electron microscope (TEM), X-ray diffraction (XRD), and energy dispersive X-ray spectroscopy (EDX), etc. We found that the addition of MnO₂ significantly increased the laccase-like activity by 300% compared to CeO₂ nanorods. Due to the excellent laccase-like activity of the MnO₂@CeO₂ nanozyme, we developed an electrochemical sensor for the detection of hazardous phenolic compounds such as bisphenol A and catechol in red wines by cyclic voltammetry (CV) and differential pulse voltammetry (DPV). We used the MnO₂@CeO₂ nanozyme to develop an electrochemical sensor for detecting harmful phenolic compounds like bisphenol A and catechol in red wine due to its excellent laccase-like activity. The MnO₂@CeO₂ nanorods could be dispersion-modified glassy carbon electrodes (GCEs) by polyethyleneimine (PEI) to achieve a rapid detection of bisphenol A and catechol, with limits of detection as low as 1.2×10^{-8} M and 7.3×10^{-8} M, respectively. This approach provides a new way to accurately determine phenolic compounds with high sensitivity, low cost, and stability.

Keywords: nanozyme; laccase; electrochemical detection; bisphenol A; catechol



Academic Editors: Montserrat Dueñas Paton and Nenadis Nikolaos

Received: 24 October 2024

Revised: 23 December 2024

Accepted: 24 December 2024

Published: 6 January 2025

Citation: Wang, C.; Wu, X.; Lin, X.; Zhu, X.; Ma, W.; Chen, J. The Electrochemical Detection of Bisphenol A and Catechol in Red Wine. *Foods* **2025**, *14*, 133. <https://doi.org/10.3390/foods14010133>

Copyright: © 2025 by the authors. Licensee MDPI, Basel, Switzerland. This article is an open access article distributed under the terms and conditions of the Creative Commons Attribution (CC BY) license (<https://creativecommons.org/licenses/by/4.0/>).

1. Introduction

Phenolic compounds in wine are known to have antioxidant properties, preventing certain diseases [1,2]. However, some phenolic substances can be harmful and affect the safety and taste of wine [3,4]. For example, bisphenol A (BPA), an endocrine disruptor, may migrate to wine from plastic packaging [5–7]. Additionally, catechol (CC) can contribute to bitter taste in wine [8]. Therefore, there is a need for a cost-effective and simple method for identifying and quantifying these harmful phenolic compounds. Traditional testing methods such as gas chromatography [9], liquid chromatography [10], and capillary electrophoresis [11] are expensive and require complex operations, limiting their application for in situ detection.

Laccase, which can catalyze the oxidation of a wide range of phenolic compounds [12–14], has been considered a candidate for detecting phenolic compounds [15,16]. However, its application has been hindered by low stability, high cost, and poor reusability [17–21]. In recent years, nanozymes, which are inorganic nanomaterials with intrinsic enzyme-like catalytic activity, have received increasing attention due to their high stability, low cost,

cyclic use, and good polyfunctionality [22–25]. Consequently, various nanomaterials have been discovered, such as carbon nanomaterials [26,27], metal (hydrogen) oxides [28,29], metal chalcogenides [30,31], and precious metal nanomaterials [32,33].

As alternatives to natural enzymes, nanozymes have been extensively utilized in biosensing, bioimaging, antimicrobial applications, antioxidant therapeutics, and environmental remediation [34]. A variety of nanozymes have been developed using metal-based elements (such as Ti, V, Cr, Mn, Fe, Co, Ni, Cu, Zn, Zr, Mo, Ru, Rh, Pd, Ag, Cd, Sn, Sb, Ce, Hf, Pt, Au, Bi), non-metal-based elements (such as C, B, Se), and their compounds or heterocomplexes [35,36]. The chemical composition (e.g., metal-based versus non-metal-based), synthesis method (e.g., impregnation, co-precipitation, deposition–precipitation, hydrothermal/solvothermal), and physical morphology (e.g., spherical, rod, cyclic, and hollow structures) each influence the properties of nanozymes in distinct ways [34]. Cerium-based nanomaterials have garnered significant attention due to their remarkable enzyme-like catalytic activity. These cerium-based nanozymes have found applications in immunoassays, analytical detection, and free radical protection owing to their high stability, low cost, ease of synthesis and modification, and biocompatibility [37,38]. Cerium oxide, a notable nanozyme, has been increasingly integrated with various nanomaterials as research advances. For instance, Bhagat et al. reported a gold-cerium dioxide core-shell structure exhibiting excellent peroxidase, catalase, and superoxide dismutase activities [39]. Additionally, Zhu et al. developed boron nitride quantum dot-anchored porous CeO₂ nanorods (BNQDs/CeO₂) that effectively catalyze the oxidation of 3,3',5,5'-tetramethylbenzidine (TMB) by H₂O₂, facilitating the detection of kanamycin in environmental and food samples [40].

Nanoceria, one of the important rare earth oxides, have recently attracted considerable interest due to their excellent redox ability, unique optical properties, and chemical stability [41–47]. Nanoceria have been reported to exhibit enzyme-like activity due to the reversible Ce³⁺/Ce⁴⁺ redox pair and oxygen vacancies on the surface [48]. Kailashiya et al. [49] explored the effects of nanoceria on human platelet functions and blood coagulation, while Singh et al. reported a remarkably active CeVO₄ nanozyme that functionally mimics cytochrome c oxidase, the terminal enzyme in the respiratory electron transport chain, by catalyzing a four-electron reduction of dioxygen to water [50]. However, most nanoceria nanozymes have focused on mimicking peroxidase [14], superoxide dismutase [51], and oxidase [52], and to date, there has been scarce study on comparing the response between this nanozyme and laccase. Several laccase-like nanozymes have been reported, including Cu/GMP as described by Hao et al. [53]. However, this system requires the removal of the solid catalyst through centrifugation post-reaction, necessitating a complex process and specialized equipment. Additionally, the CA-Cu nanozyme reported by Xu et al. exhibits poor stability under extreme pH and temperature conditions, with its catalytic performance declining significantly at pH levels below 5 or above 8 [54].

In this study, we utilized MnO₂-doped CeO₂ nanorods (CeO₂ NRs) to create hybrid nanocomposites with laccase-like activity, which were employed for detecting phenolic compounds. CeO₂ NRs with well-defined reactive planes [55,56] were easily synthesized via a solution-based hydrothermal method [57]. It has been suggested that nanorods possess higher oxidation activity than CeO₂ nanoparticles due to their more reactive planes [58]. MnO₂ was selected as a suitable dopant to modify CeO₂ NRs, resulting in MnO₂@CeO₂ NRs. The introduction of MnO₂ induced more oxygen vacancies [59], and their strong redox behavior (Ce³⁺/Ce⁴⁺ and Mn²⁺, Mn³⁺, and Mn⁴⁺) as well as the synergistic interaction between them could also accelerate oxidation reactions [60].

This study introduces an innovative approach by developing a MnO₂@CeO₂ nanozyme that mimics laccase activity, enhancing the electrochemical detection of phenolic compounds. The integration of MnO₂ into CeO₂ nanorods significantly boosts their cat-

alytic performance, increasing laccase-like activity by 300%. Leveraging this high activity, a novel electrochemical sensor was created for the rapid and sensitive detection of hazardous phenolic compounds like bisphenol A and catechol in red wine. By modifying a glassy carbon electrode with polyethyleneimine, the sensor achieves ultra-low detection limits, offering a highly sensitive, cost-effective, and stable method for food safety analysis. This method represents a significant advancement in the use of nanozymes for foodborne contaminant detection.

2. Materials and Methods

2.1. Reagents, Characterization Techniques

Ethanol, Guaiacol, 2,4-Dichlorophenol (2,4-DP) and 4-Aminoantipyrene (4-APP) were bought from Shanghai Sinopharm Chemical Reagent Co., Ltd., Shanghai, China. BPA, CC, KMnO_4 , $\text{CeCl}_3 \cdot 7\text{H}_2\text{O}$, and polyethyleneimine (PEI) were purchased from Shanghai Aladdin Biochemical Technology Co., Ltd., Shanghai, China. Exhibiting a K_m value of 0.4 mM and a V_{\max} value of 3 μM , laccase was obtained from Shanghai Yuanye Bio-Technology Co., Ltd., Shanghai, China. In this study, all chemicals were analytically pure, and the laccase used was a purified enzyme solution derived from *Trametes versicolor*. The methanol and formic acid used in the chromatographic analysis were of HPLC grade, purchased from Shanghai Macklin Biochemical Co., Ltd., Shanghai, China.

Electrochemical curves were measured by an electrochemical workstation (Chen Hua Instruments Co., Shanghai, China), using different signal transducers of cyclic voltammetry (CV) and differential pulse voltammetry (DPV). Transmission electron microscopy (TEM) images were measured by a TEM (Hitachi High-Technologies Co., Ltd., Tokyo, Japan). X-ray diffraction (XRD, Shimadzu Enterprise Management China Co., Ltd., Tokyo, Japan) patterns were recorded on the X-ray powder diffractometer. An energy dispersive spectrometer (EDS, Shanghai Jingke Scientific Instrument Co., Ltd., Shanghai, China) was used to characterize the $\text{MnO}_2@ \text{CeO}_2$ nanozyme together with TEM. Absorption spectra were performed on a UV-vis spectrophotometer (UV-1800, AoYi Instruments Shanghai Co., Ltd., Shanghai, China). An enzyme-labeled instrument was provided by Gene Co., Ltd., Hongkong, China.

2.2. Synthesis of $\text{MnO}_2@ \text{CeO}_2$ Nanozyme

The $\text{MnO}_2@ \text{CeO}_2$ nanozyme was synthesized according to a previous report with some modifications [61]. Mn^{4+} -doped CeO_2 NRs with various content of Mn^{4+} (4, 8, 12, and 16 at. %) were prepared by the hydrothermal synthesis method.

In a typical synthesis, for 8% Mn^{4+} -doped CeO_2 NRs, 0.4 g $\text{CeCl}_3 \cdot 7\text{H}_2\text{O}$ and 0.012 g KMnO_4 was dissolved in 30 mL of 9 mol/L NaOH solution under vigorous stirring. The suspension was transferred to a 50 mL Teflon-lined stainless-steel autoclave and held at 140 °C for 48 h. After the autoclave was cooled to room temperature naturally, fresh precipitates were separated by centrifugation and washed with deionized water to neutrality and with ethanol several times. The $\text{MnO}_2@ \text{CeO}_2$ nanozymes were obtained by drying the precipitates at 60 °C overnight.

2.3. Evaluation of the Catalytic Performance of Nanozyme and Laccase

The catalytic activity of the $\text{MnO}_2@ \text{CeO}_2$ nanozyme and laccase was determined using the colorimetric reaction between 2,4-DP and 4-APP; 2,4-DP (0.1 M, 10 μL) and 4-APP (0.1 M, 10 μL) was mixed with $\text{MnO}_2@ \text{CeO}_2$ nanozyme aqueous dispersion (1 mg/mL, 80 μL) or laccase (10 mg/mL, 60 μL). Then, Tris-HCl buffer (0.1 M, pH 7.0, 180 μL) was added in the mixture up to 200 μL . The reaction was maintained at 37 °C for 2 h, and then, the absorbance was detected at 485 nm.

2.4. Determination of the Catalytic Kinetic Parameters

The prepared MnO₂@CeO₂ nanozyme (1 mg/mL, 80 µL) or laccase (10 mg/mL, 60 µL) was mixed with 2,4-DP (0.1 M, 0.05, 0.1, 0.2, 0.4, 0.6, 0.8, 1.0, 2.0, 4.0, 6.0, 8.0, and 10.0 µL) and 4-APP (0.1 M, 15 µL). Tris-HCl buffer (0.1 M, pH 7.0, 180 µL) was added in the mixture up to 200 µL. At 37 °C, the kinetics of the reaction can be determined by monitoring the change in the absorption wavelength at 485 nm over time by ultraviolet-visible spectroscopy. All the experiments were repeated thrice.

The kinetic parameter was calculated via Equation (1):

$$v = \frac{V_{max}[S]}{K_m + [S]} \quad (1)$$

v is the initial velocity of the reaction, V_{max} stands for the maximal reaction velocity, K_m is the Michaelis–Menten constant, and $[S]$ is the concentration of substrate. When calculating K_m and V_{max} , the conversion form of the Michaelis–Menten equation can be used, which is named the Lineweaver–Burk Equation (2):

$$\frac{1}{v} = \frac{K_m}{V_{max}[S]} + \frac{1}{V_{max}} \quad (2)$$

2.5. Evaluation of the Stability of Catalyst

The MnO₂@CeO₂ nanozyme or laccase was incubated at varying pH (3.0–9.0) for 7 h to evaluate the effect of pH on catalytic activity. In order to study the temperature stability of the MnO₂@CeO₂ nanozyme and laccase, they were stored at –18–120 °C for 45 min before determining their catalytic activity. The catalytic activity at 30 °C was used as a reference. In the same way, the effect of organic solvents on catalytic activity was evaluated by the addition of different amounts of methanol (0, 10%, 20%, 40%, 60%, 80%, and 100% v/v) in the reactants. The absorbance of the supernatant at 485 nm was measured after 2 h.

2.6. Preparation of MnO₂@CeO₂/GCE

A total of 5 mg of MnO₂@CeO₂ nanozyme and 25 mg of PEI were added into 5 mL double distilled water and sonicated for 30 min. The GCEs were polished with 0.05 µm and 0.3 µm alumina pastes, then washed with distilled water and dried at 26 °C. A total of 5 µL of 1 mg/mL MnO₂@CeO₂ nanozyme suspension was dropped on the GCEs and then dried at room temperature. The dried modified electrode was used for the electrochemical detection of BPA and CC.

2.7. Electrochemical Experiments

A Tris buffer solution of 0.1 mol L^{−1}, pH 7.0 was used as the electrolyte solution at room temperature. A three-electrode system was formed with the MnO₂@CeO₂/GCE electrode, with the GCE electrode as the working electrode, Pt wire as the main auxiliary electrode, and Ag/AgCl as the reference electrode. The size of the electrolytic cell was 5 mL, which was purchased from Guangzhou Saios Chemical Instrument Co., Ltd., Guangzhou, China. DPV was used with a pulse amplitude of 50 mV, a pulse width of 0.05 s, a potential increment of 4 mV, a pulse cycle time of 0.5 s, a sensitivity of 1e^{−5} A V^{−1}, and a scanning in the negative direction at a potential in the range of 0.2–1.4 V with a scanning speed of 100 mV s^{−1}, and the DPV curve was recorded.

2.8. High-Performance Liquid Chromatography (HPLC) Analyses

The HPLC analysis of BPA was conducted using a HPLC instrument (Thermo Fisher UltiMate 3000, Waltham, MA, USA) equipped with a reversed-phased column Synchronis

C18 column (100 mm × 2.1 mm, 1.7 μm) maintained at a constant temperature of 30 °C with a diode array detector (DAD) set at 280 nm. The analysis involved the injection of 10 μL of 0.22 μm membrane-filtered samples at a flow rate of 0.2 mL/min, and the solvents consisted of a methanol–water mixture in a ratio of 65:35 (*v/v*).

A HPLC system (Prominence LC-20A, Shimadzu, Japan) with an analytical column Venusil MP C18 (4.6 mm × 250 mm, 5 μm) was used at a constant temperature of 35 °C. The isocratic elution was performed using a 5 mM ammonium acetate–1‰ formic acid solution (solvent A) and methanol (solvent B) in a ratio of 30:70 (*v/v*). The injection volume was 10 μL of 0.22 μm membrane-filtered samples, with a flow rate of 1 mL/min.

3. Results

3.1. Characterization of CeO₂ NRs and MnO₂@CeO₂ NRs

Figure 1 depicts TEM images of CeO₂ NRs and MnO₂@CeO₂ NRs at different scales. It can be observed that CeO₂ NRs exhibit a well-dispersed, rod-like structure with an average diameter of 8 nm. The elemental maps of Ce, Mn, and O in MnO₂@CeO₂ NRs are presented in Figure 2a–d. The maps show homogeneous distribution of O, Ce, and Mn throughout the nanorods, suggesting successful incorporation of Mn into the Ce-based nanorods. XRD was used to characterize the crystal phase of CeO₂ NRs and MnO₂@CeO₂ NRs with varying mass ratios (Figure 2e). The diffraction peaks observed at 2θ angles of 28.5°, 33.1°, 47.5°, and 56.3° correspond to the (111), (200), (220), and (311) crystalline phases. As the amount of MnO₂ increased, the diffraction peaks shifted towards the lower angle region, indicating that Mn entered the CeO₂ lattice and resulted in structural defects of CeO₂ NRs.

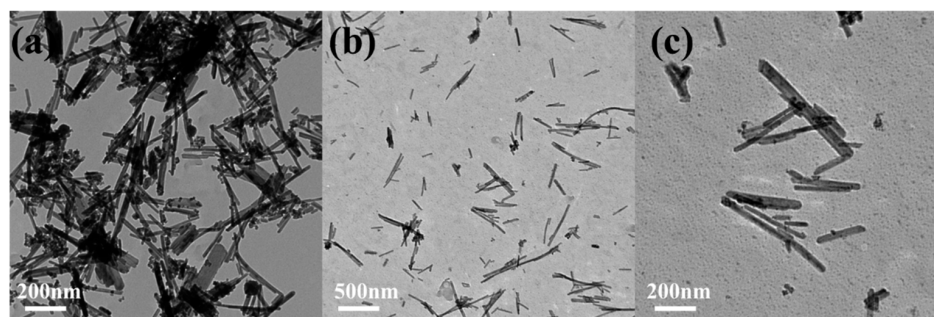


Figure 1. TEM images of (a) CeO₂, (b) MnO₂@CeO₂ (500 nm), (c) MnO₂@CeO₂ (200 nm).

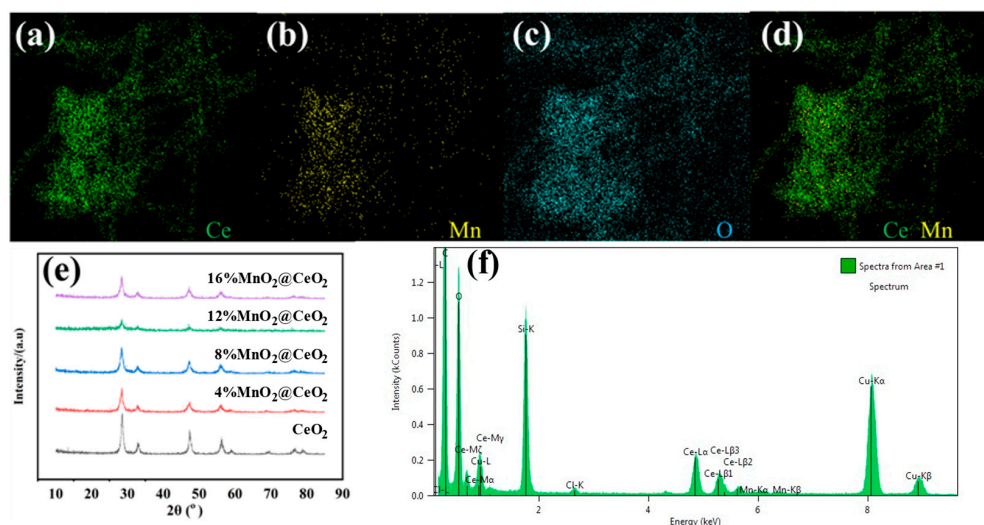


Figure 2. (a–d) Elemental mapping of MnO₂@CeO₂ NRs; (e) XRD pattern of MnO₂@CeO₂ NRs with different content of MnO₂; (f) EDX analysis of MnO₂@CeO₂ NRs.

Figure 2f presents EDX images of the synthesized nanorods, showing the presence of Mn, O, and Ce, which confirms the successful synthesis of $\text{MnO}_2@\text{CeO}_2$ NRs.

3.2. Comparison of the Catalytic Ability of $\text{MnO}_2@\text{CeO}_2$ and Laccase

The absorption spectra of various catalytic systems are presented in Figure 3. Laccase can catalyze the oxidation of 2,4-DP by simultaneously reducing molecular oxygen to water. As 2,4-DP is oxidized, the color of the solution gradually changes from colorless to red due to the reaction of the oxidation products of the phenolic pollutant with 4-APP to form a red adduct. As a result, the absorbance at 485 nm gradually increases (Figure 3, green curve). In the presence of CeO_2 NRs, 2,4-DP, and 4-APP, a similar absorption peak at 485 nm was observed, indicating the laccase-like activity. In contrast, the absorption peaks in the $\text{MnO}_2@\text{CeO}_2$ system increased by 300% compared to CeO_2 NRs, suggesting a significant enhancement of laccase-like activity. These findings imply that MnO_2 can effectively improve the catalytic activity of CeO_2 NRs. The other solutions containing the substrate without laccase or nanozyme did not show an absorption peak at 485 nm. These results confirm that the $\text{MnO}_2@\text{CeO}_2$ nanozyme possesses prominent laccase-mimicking catalytic performance.

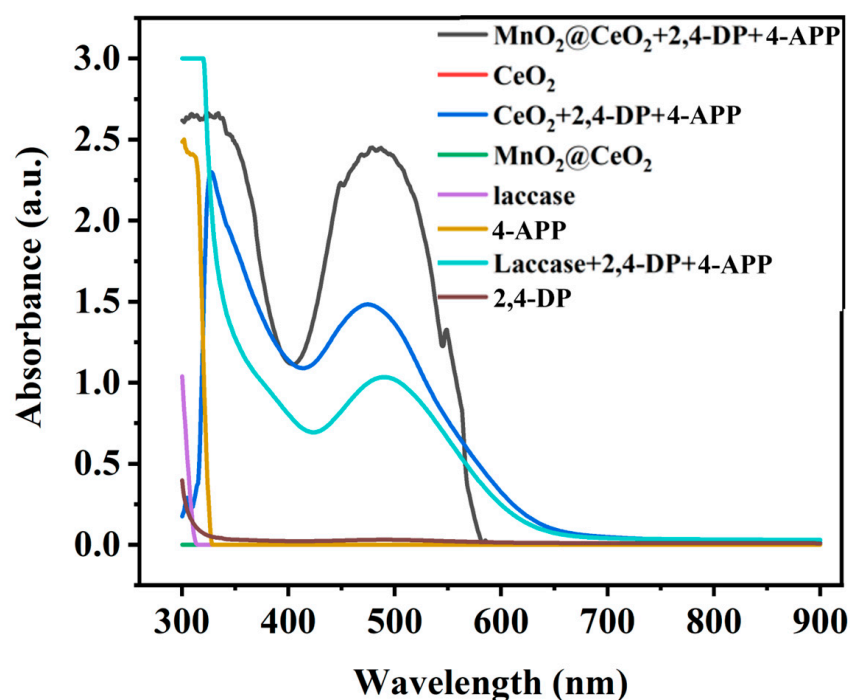


Figure 3. Absorbance spectrums of different catalytic systems.

Figure 4a shows the relative activity of the $\text{MnO}_2@\text{CeO}_2$ nanozyme with different Mn contents at pH 7.0, 20 °C and without methanol. As the Mn content was increased from 4% to 8%, a dramatic enhancement in the activity of the $\text{MnO}_2@\text{CeO}_2$ nanozyme was observed, indicating that the incorporation of MnO_2 effectively augmented the activity of the nanozymes. However, further increasing the Mn content from 8% to 16% did not yield any statistically significant differences in enzyme activity. The minor variations observed may be attributable to experimental error. Therefore, $\text{MnO}_2@\text{CeO}_2$ NRs with 8% Mn were used for the following experiments considering material consumption.

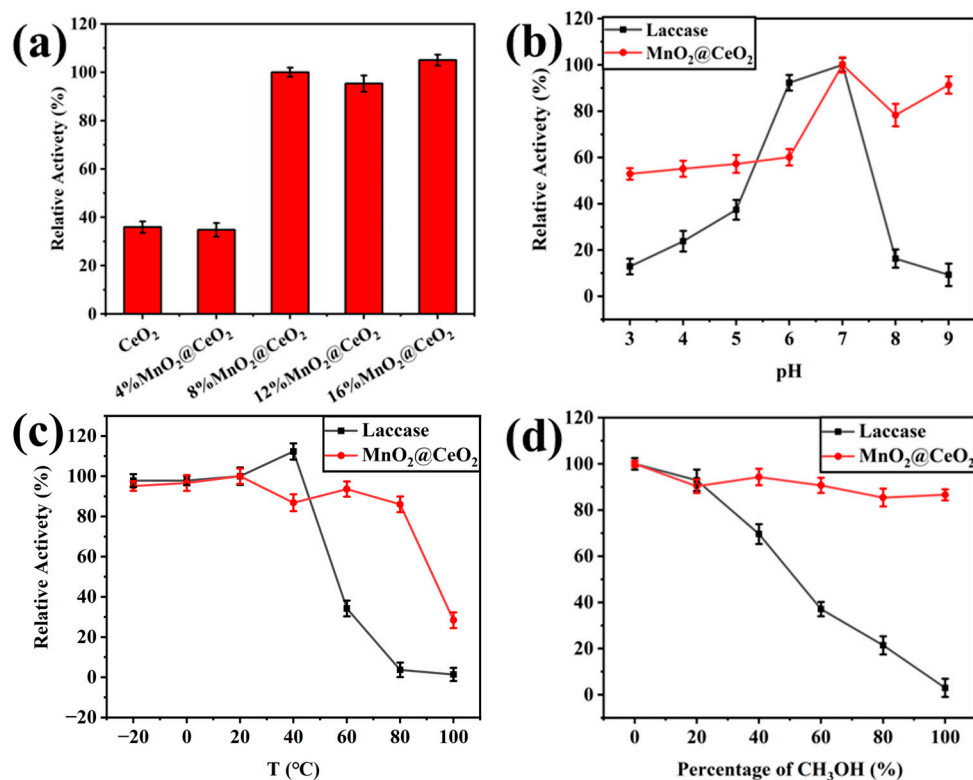


Figure 4. Relative activity of the MnO₂@CeO₂ nanozyme with increasing the content of Mn (a); relative activity of the MnO₂@CeO₂ compared with the same mass concentration of laccase at different pH (b), temperature (c), and in different CH₃OH solutions (d).

The catalytic activities of laccase and MnO₂@CeO₂ nanozyme were compared at different pH values (Figure 4b) and temperatures (Figure 4c) to verify the robust adaptability of the nanozyme. The effect of the pH value on catalytic activity was investigated at 20 °C without methanol. The catalytic activity of the laccase and MnO₂@CeO₂ nanozyme at pH 7.0 was considered as 100%, respectively. As depicted in Figure 4b, the MnO₂@CeO₂ nanozyme exhibited better catalytic activity in the range from pH 3.0 to 9.0 than laccase.

Testing at pH 7.0 without methanol, the catalytic activities of the laccase and MnO₂@CeO₂ nanozyme at 20 °C were considered as 100%, respectively. Laccase had the highest catalytic activity at 40 °C, and its activity sharply decreased as the temperature increased from 40 to 100 °C, almost becoming inactive at temperatures from 80 to 100 °C. In contrast, the relative activity of the MnO₂@CeO₂ nanozyme remained consistent from 20 to 80 °C and could still retain about 30% of the catalytic activity at 100 °C. These results indicate that the MnO₂@CeO₂ nanozyme exhibits better catalytic ability at high temperatures, as shown in Figure 4c.

To investigate the effect of organic solvent, different concentrations of methanol solution (0, 20%, 40%, 60%, 80%, and 100% *v/v*) were utilized under experimental conditions of pH 7.0 and 20 °C. As depicted in Figure 4d, the catalytic activity of laccase decreased as the methanol concentration increased. In 100% methanol solution, laccase was entirely inactivated. However, the MnO₂@CeO₂ nanozyme retained 90% of its activity in 100% methanol solution.

These results demonstrate that MnO₂@CeO₂ nanozymes have robust adaptability in different conditions.

3.3. Kinetic Parameters of NRs and Laccase

The kinetic parameters of the MnO₂@CeO₂ nanozyme and laccase were investigated by studying the oxidation of different concentrations of 2,4-DP (Figure 5). The K_m value

for the $\text{MnO}_2@\text{CeO}_2$ nanozyme was 0.7 mM, while that of laccase was 0.4 mM (shown in Table 1). The former showed nearly a 2-fold higher K_m than laccase, indicating weaker substrate-binding ability compared to the natural enzyme. Natural enzymes have flexible active sites, whereas the nanozyme is conformationally rigid. Hence, natural laccase exhibited stronger affinity towards the substrate than the $\text{MnO}_2@\text{CeO}_2$ nanozyme. The V_{\max} value of the $\text{MnO}_2@\text{CeO}_2$ nanozyme was 6 μM , while that of laccase was 3 μM , indicating a faster reaction rate for the $\text{MnO}_2@\text{CeO}_2$ nanozyme.

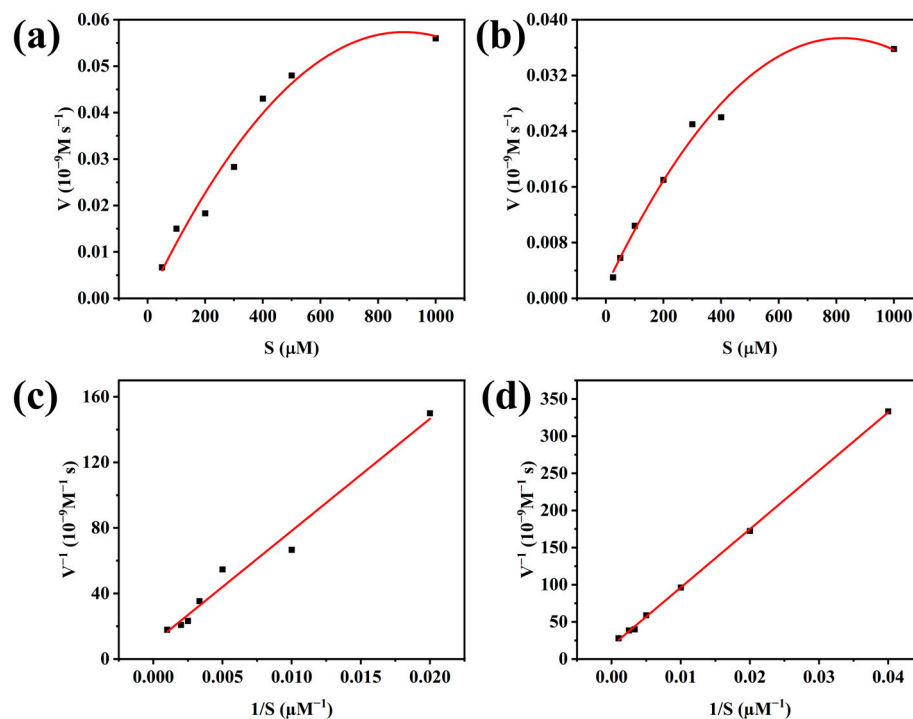


Figure 5. Steady-state kinetics of laccase (a,c) and $\text{MnO}_2@\text{CeO}_2$ nanozyme (b,d) by the catalytic oxidation with different concentrations of 2,4-DP. (c,d) are double-reciprocal plots of (a,b).

Table 1. Kinetic parameters of $\text{MnO}_2@\text{CeO}_2$ nanozyme and laccase for 2,4-DP at 37 °C.

Catalyst	K_m (mM)	V_{\max} (mM min ⁻¹)
$\text{MnO}_2@\text{CeO}_2$	0.7	6
Laccase	0.4	3

3.4. Detection of Phenols Based on $\text{MnO}_2@\text{CeO}_2/\text{GCE}$

Cyclic voltammograms of bare GCE, laccase/GCE, $\text{MnO}_2@\text{CeO}_2/\text{GCE}$, and CeO_2/GCE in 0.1 M pH 7.0 Tris containing BPA and CC at a concentration of 10^{-5} M are shown in Figure 6. The peak currents of $\text{MnO}_2@\text{CeO}_2/\text{GCE}$ for BPA and CC were much higher than those of the other electrodes, indicating excellent electrocatalytic activity of the $\text{MnO}_2@\text{CeO}_2$ nanozyme. The oxidation peaks observed in cyclic voltammograms are typically attributed to the oxidation of phenolic compounds. Specifically, laccase or nanozymes facilitate the oxidation of the hydroxyl group (-OH) in phenol, transferring electrons to molecular oxygen to generate the oxidized form of phenol (quinone) along with water. This reaction produces a signal at the electrode, which is manifested as an oxidation peak in the cyclic voltammogram.

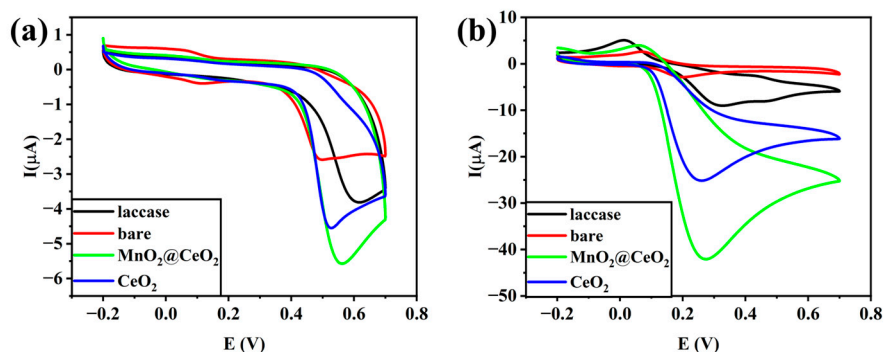


Figure 6. Cyclic voltammograms of bare GCE, laccase/GCE, $\text{MnO}_2@/\text{CeO}_2/\text{GCE}$, and CeO_2/GCE in 0.1 M pH 7.0 Tris containing BPA (a) and CC (b) with scan rate of 50 mV s^{-1} .

DPV was used for the effective detection of BPA and CC in 0.1 M Tris buffer solution with a scan rate of 0.05 v/s . Under the optimized conditions of $\text{MnO}_2@/\text{CeO}_2$ NRs shown in Figure 4, the oxidation peak current increased linearly with increasing BPA and CC concentrations (Figure 7a,b). There were linear relationships between the peak currents and the logarithm of the concentrations for BPA in the range of 4×10^{-8} to 1×10^{-4} M and for CC in the range of 2×10^{-7} to 1×10^{-4} M. The current change was also linearly correlated with the logarithm of BPA and CC concentrations within these ranges. The regression equations were $I = 1.56 \log \text{BPA} - 1.68$ ($R^2 = 0.998$), $I = 1.55 \log \text{CC} - 1.45$ ($R^2 = 0.992$). The detection limits ($S/N = 3$) for BPA and CC were 1.2×10^{-8} M and 7.3×10^{-8} M, respectively. The response time for completing a single DPV reaction is 10 s. The well-defined anodic peaks of BPA and CC indicate the excellent electrocatalytic performance of $\text{MnO}_2@/\text{CeO}_2$ nanozymes.

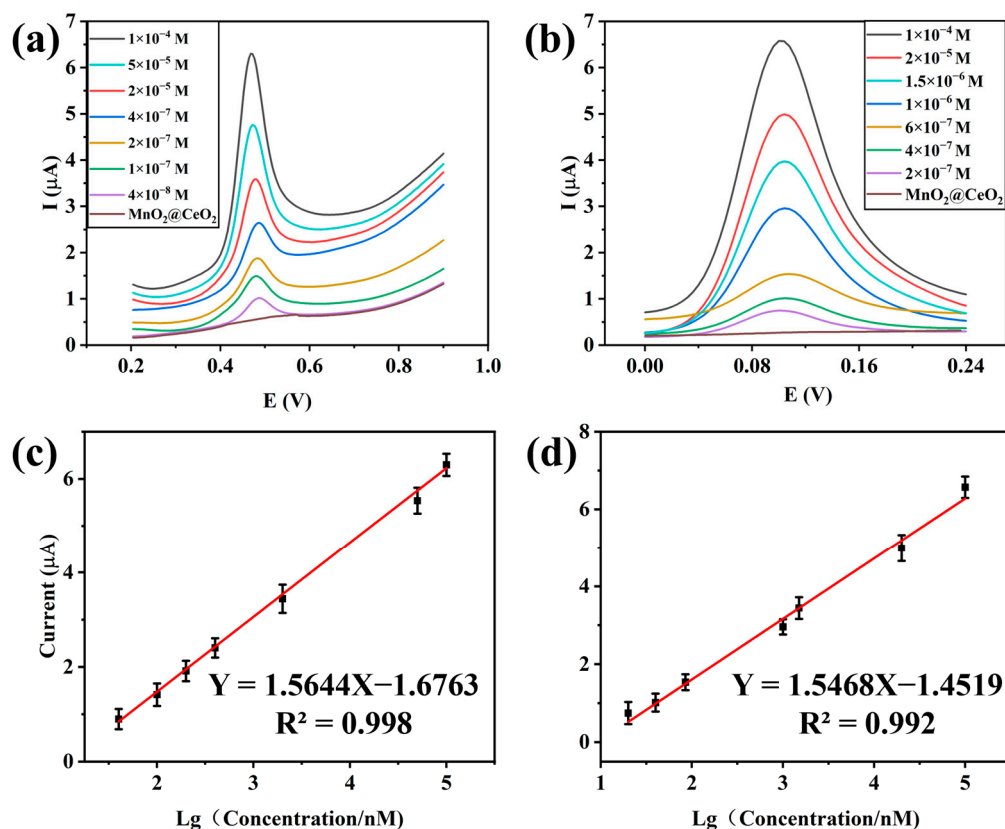


Figure 7. DPV responses of $\text{MnO}_2@/\text{CeO}_2/\text{GCE}$ with different concentrations of BPA (a) and CC (b); the linear calibration plot of BPA (c) and CC (d).

3.5. Selectivity, Reproducibility, and Stability

To investigate the selectivity of this method, some common metal ions and potential substances, including cations (K^+ , Mn^{2+} , Na^+ , Zn^{2+}), anions (Cl^- , SO_4^{2-}), glycine (Gly), urea, and glucose (Glc) were tested at concentrations 10 times higher than that of BPA and CC, which were both at 10^{-5} M. As shown in Figure 8, no significant changes were observed after the addition of interferents, indicating the high selectivity of the method.

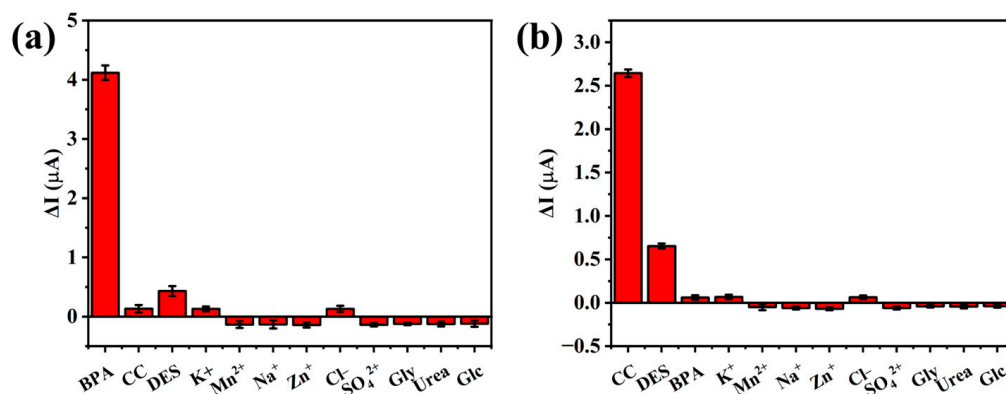


Figure 8. The selectivity of the proposed system towards BPA (a) and CC (b) detection.

In addition, we also evaluated the stability and reusability of the electrodes. First, five identical electrodes were used to test 0.1 mM BPA, and the relative standard deviation was 1.59%, indicating excellent reproducibility (Figure 9a). Subsequently, the electrode was stored at room temperature for a certain period and then used to detect 0.1 mM BPA. As shown in Figure 9b, after 14 days, the peak current decreased by only 1.86% compared to its initial value. These results demonstrate that the electrodes exhibit good stability.

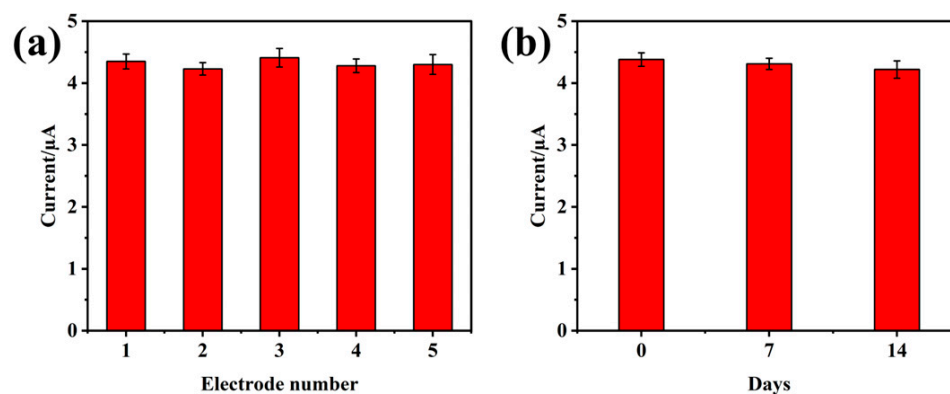


Figure 9. (a) Reproducibility and (b) stability of the electrodes.

3.6. Detection of BPA and CC in Red Wine

To evaluate the practicality of this method, red wine purchased from a supermarket was selected as a sample. Different concentrations of BPA and CC (5, 50, and 500 $\mu\text{mol/L}$, respectively) were added to the red wine, and the recoveries and relative standard deviation (RSD) were calculated (shown in Table 2). The results indicated that this method has excellent accuracy and precision and can be used for the detection of phenolic compounds in practical samples.

Table 2. Recoveries and RSD of BPA and CC in actual samples.

Analytes	Added (μM)	Found (μM)	This Work			HPLC		
			Recovery (%)	RSD (%)	Found (μM)	Recovery (%)	RSD (%)	
BPA	5	4.9	98.0	2.0	4.6	93.0	4.7	
	50	48.8	97.6	2.4	46.2	92.4	5.0	
	500	491.3	98.2	3.1	542.5	108.5	4.2	
CC	5	5.1	102.0	2.8	5.3	106.0	5.9	
	50	49.1	98.2	2.3	45.9	91.8	6.3	
	500	488.5	97.7	3.0	450.5	90.1	5.6	

4. Conclusions

In summary, the $\text{MnO}_2@\text{CeO}_2$ nanozyme with laccase-like activity was successfully prepared and exhibits excellent stability and environmental suitability under various harsh conditions compared with laccase. Furthermore, the $\text{MnO}_2@\text{CeO}_2$ nanozyme was used to fabricate a modified electrode for electrocatalytic detection, which showed good accuracy with a low detection limit and high selectivity. This work provides a novel strategy for developing electrochemical methods for the detection of phenolic compounds in practical samples based on the $\text{MnO}_2@\text{CeO}_2$ nanozyme.

Author Contributions: Conceptualization, C.W. and J.C.; methodology, X.W.; software, W.M.; validation, C.W., X.W. and X.Z.; formal analysis, C.W.; investigation, C.W.; data curation, C.W.; writing—original draft preparation, C.W.; writing—review and editing, J.C. and X.L.; supervision, J.C. and X.L.; project administration, C.W.; funding acquisition, J.C. All authors have read and agreed to the published version of the manuscript.

Funding: This work was supported by the Ningxia key research and development plan project ‘Development of Oak Barrel Substitute Material Equipment During Wine Aging’ (2022BBF01003).

Institutional Review Board Statement: Not applicable.

Informed Consent Statement: Not applicable.

Data Availability Statement: The original contributions presented in the study are included in the article; further inquiries can be directed to the corresponding author.

Conflicts of Interest: The authors declare no conflicts of interest.

References

- Duan, J.; Guo, H.; Fang, Y.; Zhou, G. The mechanisms of wine phenolic compounds for preclinical anticancer therapeutics. *Food Nutr. Res.* **2021**, *65*, 6507. [[CrossRef](#)] [[PubMed](#)]
- Muñoz-Bernal, Ó.A.; Coria-Oliveros, A.J.; de la Rosa, L.A.; Rodrigo-García, J.; del Rocío Martínez-Ruiz, N.; Sayago-Ayerdi, S.G.; Alvarez-Parrilla, E. Cardioprotective effect of red wine and grape pomace. *Food Res. Int.* **2021**, *140*, 110069. [[CrossRef](#)] [[PubMed](#)]
- Baggiani, C.; Baravalle, P.; Giovannoli, C.; Anfossi, L.; Giraudi, G. Molecularly imprinted polymer/cryogel composites for solid-phase extraction of bisphenol A from river water and wine. *Anal. Bioanal. Chem.* **2010**, *397*, 815–822. [[CrossRef](#)] [[PubMed](#)]
- Radonjić, S.; Maraš, V.; Raičević, J.; Košmerl, T. Wine or beer? Comparison, changes and improvement of polyphenolic compounds during technological phases. *Molecules* **2020**, *25*, 4960. [[CrossRef](#)] [[PubMed](#)]
- Plank, C.M.; Trela, B.C. A review of plastics use in winemaking: Haccp considerations. *Am. J. Enol. Vitic.* **2018**, *69*, 307–320. [[CrossRef](#)]
- Wang, C.; Wang, C.; Tang, K.; Rao, Z.; Chen, J. Effects of different aging methods on the phenolic compounds and antioxidant activity of red wine. *Fermentation* **2022**, *8*, 592. [[CrossRef](#)]
- Wang, J.; Yu, J.; Yu, Y.; Luo, Z.; Li, G.; Lin, X. Nanoporous electrode with stable polydimethylsiloxane coating for direct electrochemical analysis of bisphenol A in complex wine media. *Food Chem.* **2023**, *405*, 134806. [[CrossRef](#)] [[PubMed](#)]
- Salvo-Comino, C.; Martin-Pedrosa, F.; Garcia-Cabezón, C.; Rodríguez-Mendez, M.L. Silver nanowires as electron transfer mediators in electrochemical catechol biosensors. *Sensors* **2021**, *21*, 899. [[CrossRef](#)]
- Liu, Y.; Ma, C.; Zhang, Q.; Wang, W.; Pan, P.; Gu, L.; Xu, D.; Bao, J.; Dai, Z. 2D electron gas and oxygen vacancy induced high oxygen evolution performances for advanced $\text{Co}_3\text{O}_4/\text{CeO}_2$ nanohybrids. *Adv. Mater.* **2019**, *31*, 1900062. [[CrossRef](#)] [[PubMed](#)]

10. Nalewajko-Sieliwoniuk, E.; Hryniewicka, M.; Jankowska, D.; Kojło, A.; Kamianowska, M.; Szczepański, M. Dispersive liquid–liquid microextraction coupled to liquid chromatography tandem mass spectrometry for the determination of phenolic compounds in human milk. *Food Chem.* **2020**, *327*, 126996. [[CrossRef](#)] [[PubMed](#)]
11. Zhang, H.; Wu, Z.-Y.; Wang, Y.-Z.; Zhou, D.-D.; Yang, F.-Q.; Li, D.-Q. On-line immobilized trypsin microreactor for evaluating inhibitory activity of phenolic acids by capillary electrophoresis and molecular docking. *Food Chem.* **2020**, *310*, 125823. [[CrossRef](#)] [[PubMed](#)]
12. Chen, Z.; Oh, W.-D.; Yap, P.-S. Recent advances in the utilization of immobilized laccase for the degradation of phenolic compounds in aqueous solutions: A review. *Chemosphere* **2022**, *307*, 135824. [[CrossRef](#)] [[PubMed](#)]
13. Koyappayil, A.; Kim, H.T.; Lee, M.-H. ‘Laccase-like’ properties of coral-like silver citrate micro-structures for the degradation and determination of phenolic pollutants and adrenaline. *J. Hazard. Mater.* **2021**, *412*, 125211. [[CrossRef](#)] [[PubMed](#)]
14. Zhang, S.; Lin, F.; Yuan, Q.; Liu, J.; Li, Y.; Liang, H. Robust magnetic laccase-mimicking nanozyme for oxidizing o-phenylenediamine and removing phenolic pollutants. *J. Environ. Sci.* **2020**, *88*, 103–111. [[CrossRef](#)] [[PubMed](#)]
15. Lou, C.; Jing, T.; Zhou, J.; Tian, J.; Zheng, Y.; Wang, C.; Zhao, Z.; Lin, J.; Liu, H.; Zhao, C. Laccase immobilized polyaniline/magnetic graphene composite electrode for detecting hydroquinone. *Int. J. Biol. Macromol.* **2020**, *149*, 1130–1138. [[CrossRef](#)] [[PubMed](#)]
16. Othman, A.M.; Wollenberger, U. Amperometric biosensor based on coupling aminated laccase to functionalized carbon nanotubes for phenolics detection. *Int. J. Biol. Macromol.* **2020**, *153*, 855–864. [[CrossRef](#)]
17. Ladole, M.R.; Pokale, P.B.; Patil, S.S.; Belokar, P.G.; Pandit, A.B. Laccase immobilized peroxidase mimicking magnetic metal organic frameworks for industrial dye degradation. *Bioresour. Technol.* **2020**, *317*, 124035. [[CrossRef](#)] [[PubMed](#)]
18. Liu, M.; Wang, C.; Ren, X.; Gao, S.; Yu, S.; Zhou, J. Remodelling metabolism for high-level resveratrol production in *Yarrowia lipolytica*. *Bioresour. Technol.* **2022**, *365*, 128178. [[CrossRef](#)]
19. Singh, G.; Arya, S.K. Utility of laccase in pulp and paper industry: A progressive step towards the green technology. *Int. J. Biol. Macromol.* **2019**, *134*, 1070–1084. [[CrossRef](#)] [[PubMed](#)]
20. Wang, C.; Ma, W.; Xu, L.; Wei, Z.; Tang, K.; Zhou, J.; Chen, J. Integrative metabolic and cellular organelle engineering for improving biosynthesis of flavonoid compounds in *saccharomyces cerevisiae*. *Food Biosci.* **2024**, *60*, 103996. [[CrossRef](#)]
21. Wang, M.; Wang, S.; Song, X.; Liang, Z.; Su, X. Photo-responsive oxidase mimic of conjugated microporous polymer for constructing a pH-sensitive fluorescent sensor for bio-enzyme sensing. *Sens. Actuators B Chem.* **2020**, *316*, 128157. [[CrossRef](#)]
22. Ding, H.; Hu, B.; Zhang, B.; Zhang, H.; Yan, X.; Nie, G.; Liang, M. Carbon-based nanozymes for biomedical applications. *Nano Res.* **2021**, *14*, 570–583. [[CrossRef](#)]
23. Li, S.; Shang, L.; Xu, B.; Wang, S.; Gu, K.; Wu, Q.; Sun, Y.; Zhang, Q.; Yang, H.; Zhang, F. A nanozyme with photo-enhanced dual enzyme-like activities for deep pancreatic cancer therapy. *Angew. Chem.* **2019**, *131*, 12754–12761. [[CrossRef](#)]
24. Mao, M.; Guan, X.; Wu, F.; Ma, L. CoO nanozymes with multiple catalytic activities regulate atopic dermatitis. *Nanomaterials* **2022**, *12*, 638. [[CrossRef](#)] [[PubMed](#)]
25. Portorreal-Bottier, A.; Gutiérrez-Tarriño, S.; Calvente, J.J.; Andreu, R.; Roldán, E.; Oña-Burgos, P.; Olloqui-Sariego, J.L. Enzyme-like activity of cobalt-MOF nanosheets for hydrogen peroxide electrochemical sensing. *Sens. Actuators B Chem.* **2022**, *368*, 132129. [[CrossRef](#)]
26. Li, Y.; Cui, R.; Huang, H.; Dong, J.; Liu, B.; Zhao, D.; Wang, J.; Wang, D.; Yuan, H.; Guo, X. High performance determination of Pb²⁺ in water by 2, 4-dithiobiuret-reduced graphene oxide composite with wide linear range and low detection limit. *Anal. Chim. Acta* **2020**, *1125*, 76–85. [[CrossRef](#)] [[PubMed](#)]
27. Zhou, X.; Deng, J.; Yang, R.; Zhou, D.; Fang, C.; He, X.; Wang, D.; Lei, W.; Hu, J.; Li, Y. Facile preparation and characterization of fibrous carbon nanomaterial from waste polyethylene terephthalate. *Waste Manag.* **2020**, *107*, 172–181. [[CrossRef](#)] [[PubMed](#)]
28. Sun, Y.; Chen, M.; Liu, H.; Zhu, Y.; Wang, D.; Yan, M. Adsorptive removal of dye and antibiotic from water with functionalized zirconium-based metal organic framework and graphene oxide composite nanomaterial UiO-66-(OH)₂/GO. *Appl. Surf. Sci.* **2020**, *525*, 146614. [[CrossRef](#)]
29. Tabassum, R.; Kant, R. Recent trends in surface plasmon resonance based fiber–optic gas sensors utilizing metal oxides and carbon nanomaterials as functional entities. *Sens. Actuators B Chem.* **2020**, *310*, 127813. [[CrossRef](#)]
30. Han, J.; Zou, Q.; Su, W.; Yan, X. Minimal metallo-nanozymes constructed through amino acid coordinated self-assembly for hydrolase-like catalysis. *Chem. Eng. J.* **2020**, *394*, 124987. [[CrossRef](#)]
31. Wei, D.; Zhang, X.; Chen, B.; Zeng, K. Using bimetallic Au@ Pt nanozymes as a visual tag and as an enzyme mimic in enhanced sensitive lateral-flow immunoassays: Application for the detection of streptomycin. *Anal. Chim. Acta* **2020**, *1126*, 106–113. [[CrossRef](#)]
32. Ko, E.; Tran, V.-K.; Son, S.E.; Hur, W.; Choi, H.; Seong, G.H. Characterization of Au@ PtNP/GO nanozyme and its application to electrochemical microfluidic devices for quantification of hydrogen peroxide. *Sens. Actuators B Chem.* **2019**, *294*, 166–176. [[CrossRef](#)]
33. Liu, B.; Liu, J. Sensors and biosensors based on metal oxide nanomaterials. *TrAC Trends Anal. Chem.* **2019**, *121*, 115690. [[CrossRef](#)]
34. Wang, H.; Wan, K.; Shi, X. Recent advances in nanozyme research. *Adv. Mater.* **2019**, *31*, 1805368. [[CrossRef](#)]

35. Wei, H.; Wang, E. Nanomaterials with enzyme-like characteristics (nanozymes): Next-generation artificial enzymes. *Chem. Soc. Rev.* **2013**, *42*, 6060–6093. [[CrossRef](#)] [[PubMed](#)]
36. Wu, J.; Wang, X.; Wang, Q.; Lou, Z.; Li, S.; Zhu, Y.; Qin, L.; Wei, H. Nanomaterials with enzyme-like characteristics (nanozymes): Next-generation artificial enzymes (II). *Chem. Soc. Rev.* **2019**, *48*, 1004–1076. [[CrossRef](#)] [[PubMed](#)]
37. Dong, S.; Dong, Y.; Jia, T.; Liu, S.; Liu, J.; Yang, D.; He, F.; Gai, S.; Yang, P.; Lin, J. GSH-depleted nanozymes with hyperthermia-enhanced dual enzyme-mimic activities for tumor nanocatalytic therapy. *Adv. Mater.* **2020**, *32*, 2002439. [[CrossRef](#)] [[PubMed](#)]
38. Liu, Z.; Wang, F.; Ren, J.; Qu, X. A series of MOF/Ce-based nanozymes with dual enzyme-like activity disrupting biofilms and hindering recolonization of bacteria. *Biomaterials* **2019**, *208*, 21–31. [[CrossRef](#)] [[PubMed](#)]
39. Bhagat, S.; Vallabani, N.S.; Shutthanandan, V.; Bowden, M.; Karakoti, A.S.; Singh, S. Gold core/ceria shell-based redox active nanozyme mimicking the biological multienzyme complex phenomenon. *J. Colloid Interface Sci.* **2018**, *513*, 831–842. [[CrossRef](#)]
40. Zhu, X.; Tang, L.; Wang, J.; Peng, B.; Ouyang, X.; Tan, J.; Yu, J.; Feng, H.; Tang, J. Enhanced peroxidase-like activity of boron nitride quantum dots anchored porous CeO₂ nanorods by aptamer for highly sensitive colorimetric detection of kanamycin. *Sens. Actuators B Chem.* **2021**, *330*, 129318. [[CrossRef](#)]
41. Chen, L.-N.; Hou, K.-P.; Liu, Y.-S.; Qi, Z.-Y.; Zheng, Q.; Lu, Y.-H.; Chen, J.-Y.; Chen, J.-L.; Pao, C.-W.; Wang, S.-B. Efficient hydrogen production from methanol using a single-site Pt₁/CeO₂ catalyst. *J. Am. Chem. Soc.* **2019**, *141*, 17995–17999. [[CrossRef](#)] [[PubMed](#)]
42. Chen, Y.; Liu, Y.; Guo, C.; Yin, C.; Xie, C.; Fan, Q. Self-Amplified Competitive Coordination of MnO₂-Doped CeO₂ Nanozyme for Synchronously Activated Combination Therapy. *Adv. Funct. Mater.* **2023**, *33*, 2209927. [[CrossRef](#)]
43. Chen, Y.; Liu, Y.; Kuang, P.; Guo, C.; Zan, J.; Xie, C.; Yin, C.; Fan, Q. Tumor microenvironment activated nanoenzyme-based agents for enhanced MRI-guided photothermal therapy in the NIR-II window. *Chem. Commun.* **2022**, *58*, 2742–2745. [[CrossRef](#)] [[PubMed](#)]
44. Chen, Y.; Zan, J.; Liu, Y.; Kuang, P.; Guo, C.; Xie, C.; Huang, W.; Fan, Q. A cerium oxide-based nanomedicine for pH-triggered chemodynamic/chemo combination therapy. *J. Mater. Chem. B* **2022**, *10*, 1403–1409. [[CrossRef](#)] [[PubMed](#)]
45. Liu, L.; Meng, W.-K.; Li, L.; Xu, G.-J.; Wang, X.; Chen, L.-Z.; Wang, M.-L.; Lin, J.-M.; Zhao, R.-S. Facile room-temperature synthesis of a spherical mesoporous covalent organic framework for ultrasensitive solid-phase microextraction of phenols prior to gas chromatography-tandem mass spectrometry. *Chem. Eng. J.* **2019**, *369*, 920–927. [[CrossRef](#)]
46. Ma, B.; Han, J.; Zhang, K.; Jiang, Q.; Sui, Z.; Zhang, Z.; Zhao, B.; Liang, Z.; Zhang, L.; Zhang, Y. Targeted killing of tumor cells based on isoelectric point suitable nanoceria-rod with high oxygen vacancies. *J. Mater. Chem. B* **2022**, *10*, 1410–1417. [[CrossRef](#)]
47. Mehta, A.; Scammon, B.; Shrake, K.; Bredikhin, M.; Gil, D.; Shekunova, T.; Baranchikov, A.; Ivanov, V.; Reukov, V. Nanoceria: Metabolic interactions and delivery through PLGA-encapsulation. *Mater. Sci. Eng. C* **2020**, *114*, 111003. [[CrossRef](#)]
48. Ma, Y.; Tian, Z.; Zhai, W.; Qu, Y. Insights on catalytic mechanism of CeO₂ as multiple nanozymes. *Nano Res.* **2022**, *15*, 10328–10342. [[CrossRef](#)]
49. Kailashiya, J.; Dash, D. Effects of nanoceria on human platelet functions and blood coagulation. *Int. J. Nanomed.* **2022**, *17*, 273–284. [[CrossRef](#)] [[PubMed](#)]
50. Singh, N.; Muges, G. CeVO₄ nanozymes catalyze the reduction of dioxygen to water without releasing partially reduced oxygen species. *Angew. Chem. Int. Ed.* **2019**, *58*, 7797–7801. [[CrossRef](#)] [[PubMed](#)]
51. Zhou, X.; Zeng, W.; Rong, S.; Lv, H.; Chen, Y.; Mao, Y.; Tan, W.; Li, H. Alendronate-modified nanoceria with multi-antioxidant enzyme-mimetic activity for reactive oxygen species/reactive nitrogen species scavenging from cigarette smoke. *ACS Appl. Mater. Interfaces* **2021**, *13*, 47394–47406. [[CrossRef](#)] [[PubMed](#)]
52. Kim, H.Y.; Park, K.S.; Park, H.G. Glucose oxidase-like activity of cerium oxide nanoparticles: Use for personal glucose meter-based label-free target DNA detection. *Theranostics* **2020**, *10*, 4507. [[CrossRef](#)]
53. Liang, H.; Lin, F.; Zhang, Z.; Liu, B.; Jiang, S.; Yuan, Q.; Liu, J. Multicopper laccase mimicking nanozymes with nucleotides as ligands. *ACS Appl. Mater. Interfaces* **2017**, *9*, 1352–1360. [[CrossRef](#)] [[PubMed](#)]
54. Xu, X.; Wang, J.; Huang, R.; Qi, W.; Su, R.; He, Z. Preparation of laccase mimicking nanozymes and their catalytic oxidation of phenolic pollutants. *Catal. Sci. Technol.* **2021**, *11*, 3402–3410. [[CrossRef](#)]
55. Han, S.I.; Lee, S.w.; Cho, M.G.; Yoo, J.M.; Oh, M.H.; Jeong, B.; Kim, D.; Park, O.K.; Kim, J.; Namkoong, E. Epitaxially strained CeO₂/Mn₃O₄ nanocrystals as an enhanced antioxidant for radioprotection. *Adv. Mater.* **2020**, *32*, 2001566. [[CrossRef](#)]
56. Salvo-Comino, C.; Rassas, I.; Minot, S.; Bessueille, F.; Rodriguez-Mendez, M.L.; Errachid, A.; Jaffrezic-Renault, N. Voltammetric sensor based on electrodeposited molecularly imprinted chitosan film on BDD electrodes for catechol detection in buffer and in wine samples. *Mater. Sci. Eng. C* **2020**, *110*, 110667. [[CrossRef](#)]
57. Hancock, M.L.; Yokel, R.A.; Beck, M.J.; Calahan, J.L.; Jarrells, T.W.; Munson, E.J.; Olaniyan, G.A.; Grulke, E.A. The characterization of purified citrate-coated cerium oxide nanoparticles prepared via hydrothermal synthesis. *Appl. Surf. Sci.* **2021**, *535*, 147681. [[CrossRef](#)]
58. Zhang, J.; Tan, Z.; Leng, W.; Chen, Y.-C.; Zhang, S.; Lo, B.T.; Yung, K.K.L.; Peng, Y.-K. Chemical state tuning of surface Ce species on pristine CeO₂ with 2400% boosting in peroxidase-like activity for glucose detection. *Chem. Commun.* **2020**, *56*, 7897–7900. [[CrossRef](#)]

59. Zhang, X.; Yang, P.; Liu, Y.; Pan, J.; Li, D.; Wang, B.; Feng, J. Support morphology effect on the selective oxidation of glycerol over AuPt/CeO₂ catalysts. *J. Catal.* **2020**, *385*, 146–159. [[CrossRef](#)]
60. Jampaiah, D.; Velisoju, V.K.; Devaiah, D.; Singh, M.; Mayes, E.L.; Coyle, V.E.; Reddy, B.M.; Bansal, V.; Bhargava, S.K. Flower-like Mn₃O₄/CeO₂ microspheres as an efficient catalyst for diesel soot and CO oxidation: Synergistic effects for enhanced catalytic performance. *Appl. Surf. Sci.* **2019**, *473*, 209–221. [[CrossRef](#)]
61. Wu, Q.; Zhang, F.; Xiao, P.; Tao, H.; Wang, X.; Hu, Z.; Lu, Y. Great influence of anions for controllable synthesis of CeO₂ nanostructures: From nanorods to nanocubes. *J. Phys. Chem. C* **2008**, *112*, 17076–17080. [[CrossRef](#)]

Disclaimer/Publisher's Note: The statements, opinions and data contained in all publications are solely those of the individual author(s) and contributor(s) and not of MDPI and/or the editor(s). MDPI and/or the editor(s) disclaim responsibility for any injury to people or property resulting from any ideas, methods, instructions or products referred to in the content.